
UNIVERSITY OF BIRMINGHAM

UF
UNIVERSITY of FLORIDA

# Investigation of beam clipping in the Power Recycling Cavity of Advanced LIGO using FINESSE

Charlotte Bond, Paul Fulda, Daniel Brown and Andreas Freise

LIGO DCC: T1300954

*Issue:* 1
*Date:* December 16, 2013

School of Physics and Astronomy
University of Birmingham
Birmingham, B15 2TT

University of Florida
Department of Physics
Gainesville, FL32611-8440

# Contents



# 1 Introduction

This note documents preliminary investigations using FINESSE[1] [1] into possible causes of the observed reduction in power recycling gain in the L1 power recycled Michelson interferometer (PRMI) [2]. This note aims to describe the evidence from measurements made on site, to record the methods and results of the simulation effort, and to suggest a conclusion for the likely cause of the observed reduction in circulating light power.

**Preliminary conclusion:** the observed power build up can be explained largely by considering the greater than expected clipping at the central beam-splitter, due to the larger beam-sizes in the power recycling cavity; see figure 1 for the measured data and figures 7 and 11 for the simulation results.

## 1.1 State of the L1 power recycled Michelson

During the installation and commissioning of the L1 OMC, it was observed that the output mode from the PRMI did not match as well to the OMC eigenmode as expected [4]. It was also observed that the X-arm mode did not match well to the Y-arm mode. The leading candidate for causing the difference between X-arm and Y-arm modes was identified as asymmetry between the ITMX and ITMY substrates [5].

Measurements performed by the polisher identified discrepancies between the wavefront curvature of light reflected from the HR surface of the ITM optics via the AR surface, and the expected wavefront curvature calculated from the measured radius of curvature of the HR surface itself [6, 7]. This indicates the presence of ITM *non-thermal* substrate lenses. These ITM substrate lens focal lengths were calculated to be 305 km and -82.4 km for the ITMX and ITMY substrates respectively.

[1] Note that some of the files make use of new features available at the time of writing in the 'develop' branch on the git repository hosting the FINESSE source code.

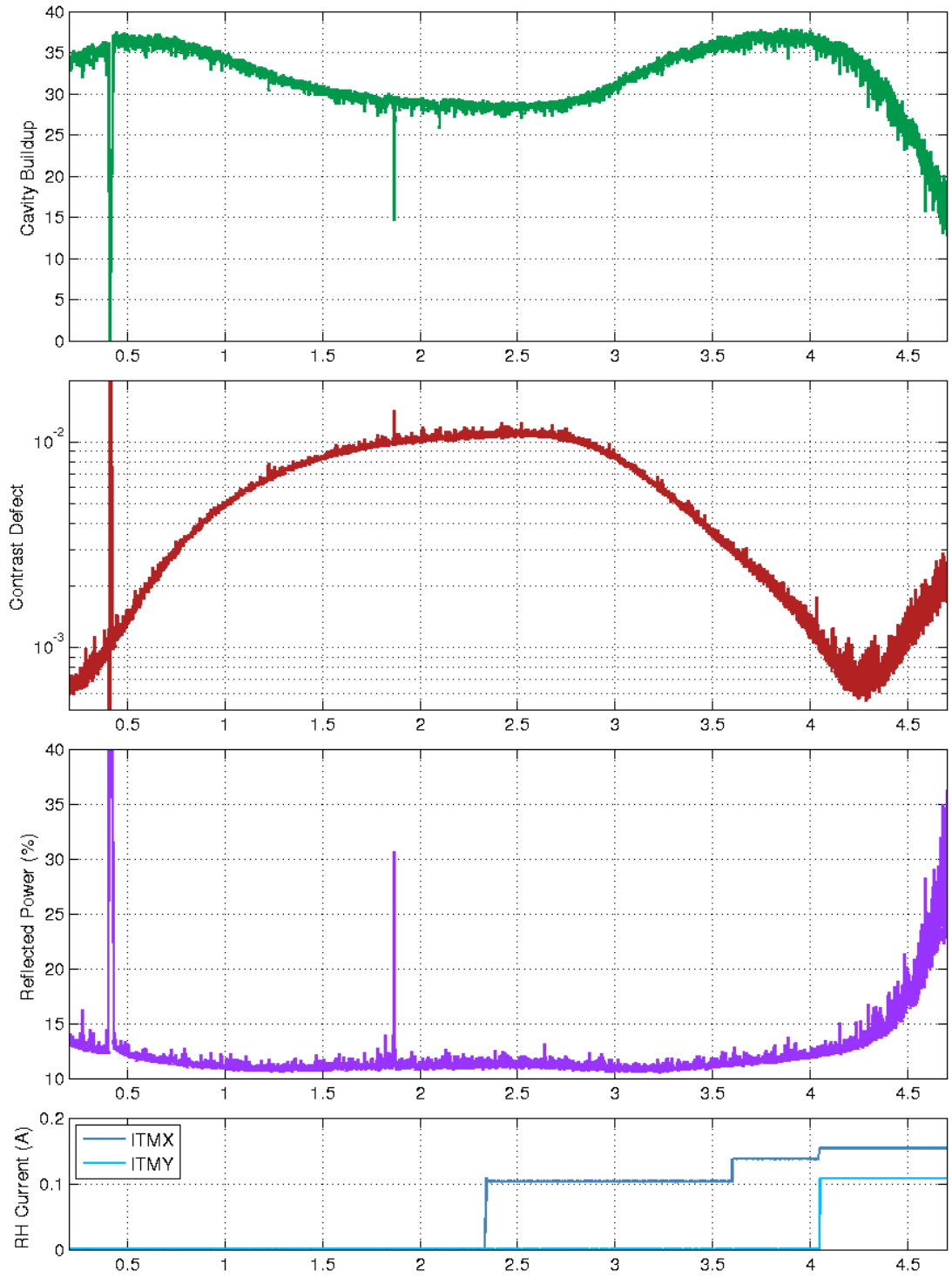


Figure 1: Plots showing (from top to bottom) the power build up in the PRC, contrast defect, reflected power and the current applied to the ring-heaters on the ITMs over time. At time 0 the ITMX ring heater is switched off. At around 2 hours ITMX has cooled down and the ITMX ring heater is switched back on. At ∼4 hours the ring heater on ITMY is switched on. Image courtesy of Denis Martynov and Chris Mueller [3].

### 1.2 Observed power recycling gain

In order to better match the X and Y arms of the PRMI, the ITMX ring heater was actuated, creating a negative thermal lens in the ITMX substrate. This was observed to reduce the contrast defect and to increase the power recycling gain, as expected. However, even at its maximum of around 37, the observed power recycling gain was significantly lower than the expected factor of 58 calculated from the aLIGO design parameters (see Fig. 1 taken from LLO aLOG entry 9733 [3]). Also noteworthy is the fact that the x-axis position of the maximum in power recycling gain does not correspond with the x-axis position of the minimum in contrast defect.

### 1.3 Optical parameters used in the simulation

The L1 PRMI model file used throughout this investigation is derived from the full L1 core interferometer FINESSE file, which can be found on the DCC [8]. The file incorporates all optical surfaces from the HR surface of the PRM to the AR surface of the SRM, including all PR optics, a thick central beam splitter, thick ITMs including both non-thermal lenses and the option for a thermal lens, all SR optics and a thick SRM.

For this investigation the optical parameters (reflection coefficients, losses etc.) and geometric properties (radii of curvature, thickness etc.) are the current measurements of the cold optics installed at L1, recorded in [11]. All distances between optics are taken from the L1 Master coordinate list [12].

Several parameters in this investigation are varied from their measured values in the references listed above. Where indicated, these parameters are varied while maintaining the other geometric and optical properties as recorded in [11] and [12]. These varied parameters include:

- Radii of curvature of the ITMs, to simulate the actuation of the ring heaters.
- Radius of curvature of PR3, to investigate the effects of possible errors in the measured $R_c$.
- Centering of the beam on the beam splitter.

For all simulations reported in this note the ITM thermal lenses are considered to have infinite focal length (low power operation without arm cavities). The effect of the ring heaters is modelled simply as a change in radius of curvature of ITMs. This is a reasonable approximation to the actual effect of the ring heater in this case because the Gouy phase separation between the ITM HR surface and the substrate thermal lens equivalent location is negligible.

## 2 Simulations without modelling beam clipping

Before considering the effects of finite apertures, we looked at the power recycling gain, contrast defect, and reflected light power in an L1 PRMI-like interferometer with optics of effectively infinite radius. We also investigated the expected beam sizes at the beam splitter location as a motivation for studying clipping effects in the PRMI more closely (see section 3).

### 2.1 PRMI power budget without clipping

The first check performed with the FINESSE file for the L1 PRMI was to predict the power recycling gain, reflected power and contrast defect in a plane-wave approximation. The only losses taken into account in this simulation are those directly measured from the individual optics, i.e. losses due to absorption, scattering, pick-off transmissions and AR coating reflectivity, the values for all of which are taken from [11]. In the plane wave approximation model, the power recycling gain was 53, the contrast defect was $\sim 10^{-8}$ and the reflected power was 13.7 % of the input power. Here we already see a reduction of ∼5 in the power recycling gain from the expected value 58, purely as a consequence of including the measured losses.

Next we moved from the plane wave model to a model including Gaussian beam tracing and the potential for mode mismatches between the X and Y arm. The ITMX radius of curvature was varied to simulate the effects of actuating the ring heater. Allowing the input beam to match to the PRY cavity the maximum PRC gain was achieved with the closest mode-match between the two arms, at ITMX $R_c \sim 1901.5$ m (compared to the cold value of -1938 m). The observed values of PRC gain, contrast defect and reflected power with this arm mode-match were similar to those of the plane wave model. The model was adapted for an input beam

mode-mismatched to both PRX and PRY, instead taking the beam which would match the ideal L1 design in the presence of 50 km thermal lenses in the ITMs. This is our best guess of the mode coming from the PMMT optics. The maximum power recycling gain achieved in this model was still 52, significantly higher than the value of 37 observed in the experiment. The minimum contrast defect increased to $\sim 10^{-7}$, and the maximum reflected power to 14.8 % of the input light power. A model with a larger initial mode mismatch was tried, but in the case where the mode mismatch was large enough to bring the power recycling gain significantly lower than 50, the reflected light power was much higher than 15 %, thus disagreeing with the observations.

The result that mode mismatches alone could not account for the observed drop in power recycling gain motivated an investigation into the beam sizes in the core interferometer as a function of ITMX radius of curvature, with the view to including possible clipping at the beam splitter in the model.

## 2.2 Beam sizes at the beam splitter

The beam parameters in the central interferometer are crucial in determining the mode-mismatch losses as well as clipping losses at the beam splitter and other core optics.

At the time of writing this note the as-built L1 interferometer geometry is expected to deviate from the original optimised design in several ways which are important for this investigation:

- The presence of ITM substrate lenses due to substrate imhomogeneity [6, 7]. The focal lengths of these lenses have been calculated to be -82.4 km for ITMY and +305 km for ITMX.
- At low-power operation, the ITMs have no substrate thermal lens present. The geometrical design of the stable recycling cavities was optimised for low power operation (∼12.5 W input power) which is expected to give rise to +50 km focal length lenses in the ITM substrates [9].
- The measurement error bars on the radii of curvature of the power recycling optics, as well as the uncertainty in their exact placement on the HAM tables, allow for a range of possible power recycling cavity eigenmode beam parameters.

The ITM substrate non-thermal lenses are the principle reason that the ring heaters are currently being used in the L1 interferometer. Without using the ring heaters to match the X and Y arm geometries, the contrast defect is large ($\sim$ 1 %) due to the difference in beam parameters of the two arms at the beam splitter. This case, where the ITMs are cold, occurs at around the 2 hour mark in figure 1.

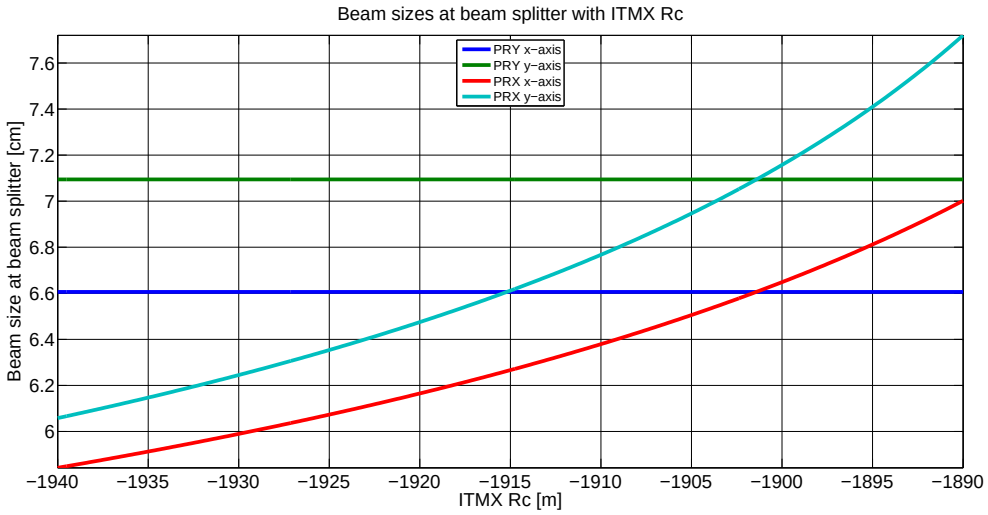


Figure 2: Beam sizes at the beam splitter HR surface for different ITMX radii of curvature, with all other optics parameters as specified in section 1.3. In the L1 interferometer the ITMX ring heater has been used to tune the PRX beam size to match the PRY beam size.

For the power recycled Michelson interferometer with no arm cavities, the dominant effect of actuating the ring heater is to create a negative thermal lens in the ITM substrate [10]. Thus it can be seen that in order

to match the X and Y arms, it is necessary to actuate only on the ITMX ring heater in order to change the ITMX substrate thermal lens from +305 km to -82.4 km. This has the effect of pushing the power recycling cavity geometry even further away from the optimised design, since the optimised design considered both ITMs to have a substrate thermal lens of +50 km.

Figure 2 shows how the beam sizes at the central beam splitter vary with the radius of curvature of ITMX in our model of the L1 central interferometer. These beam sizes can be compared against the expected beam sizes of ∼5.3 cm for the L1 interferometer design with as-built power recycling optics, matching ITM radii of curvature, no ITM substrate non-thermal lenses, and +50 km ITM substrate thermal lenses [9].

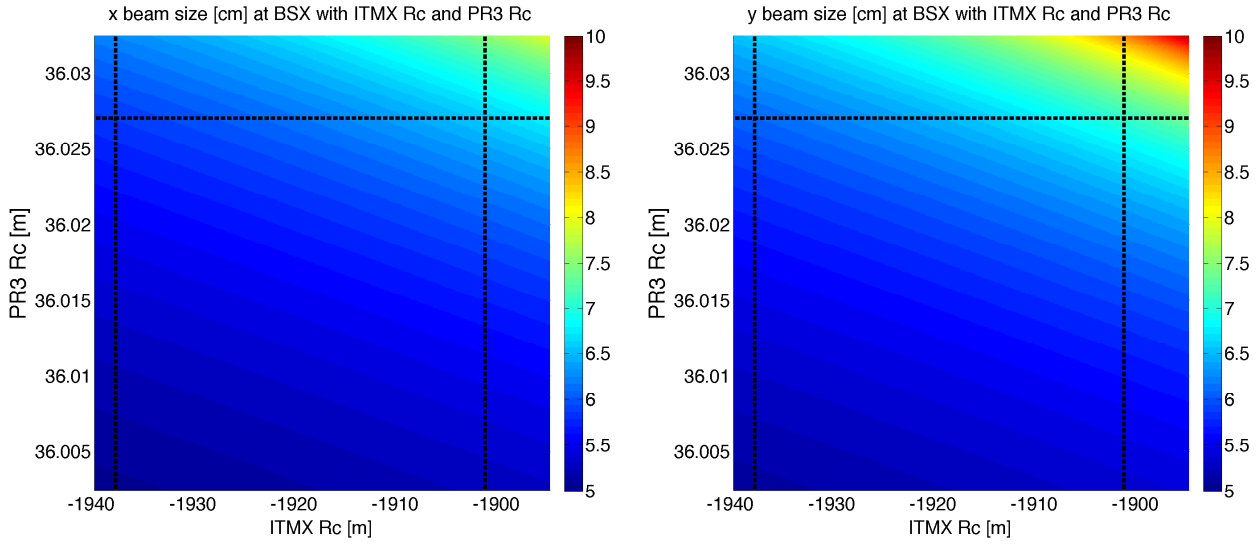


Figure 3: Beam sizes at the beam splitter HR surface for different PR3 and ITMX radii of curvature. All other optics parameters are as specified in section 1.3. The horizontal line shows the nominal PR3 radius of curvature from [11]. The left-hand vertical line shows the nominal ITMX radius of curvature without ring heater actuation, and the right-hand vertical line shows the ITMX radius of curvature when matched to the Y arm.

Finally, we consider the effect of errors in the as-built power recycling cavity optics on the beam size at the beam splitter. It is known that the most sensitive aspect of the power recycling cavity with regards to determining the beam size at the beam splitter is the distance between PR2 and PR3 compared to the focal length of PR3 (half the radius of curvature of PR3). We found it sufficient to observe the variation in beam size at the beam splitter with PR3 radius of curvature. It is worth mentioning for clarity that unless the PR3 radius of curvature is explicitly being varied as part of the investigation, we use the value of 36.027 m provided on the LIGO optics reference page [11].

Figure 3 shows the PRX beam sizes along the x and y-axes at the beam splitter as a function of PR3 and ITMX radii of curvature. This figure shows that if the PR3 radius of curvature is longer than the measured value by just a few mm, the beam size at the beam splitter can increase by several mm. The effect of increasing the radius of curvature of PR3 becomes more dramatic as the ITMX radius of curvature is reduced, as is caused by actuating the ITMX ring heater.

# 3 Modelling beam clipping effects

In the following we present the results for simulations that include the additional optical losses due to beam clipping at the central beam-splitter.

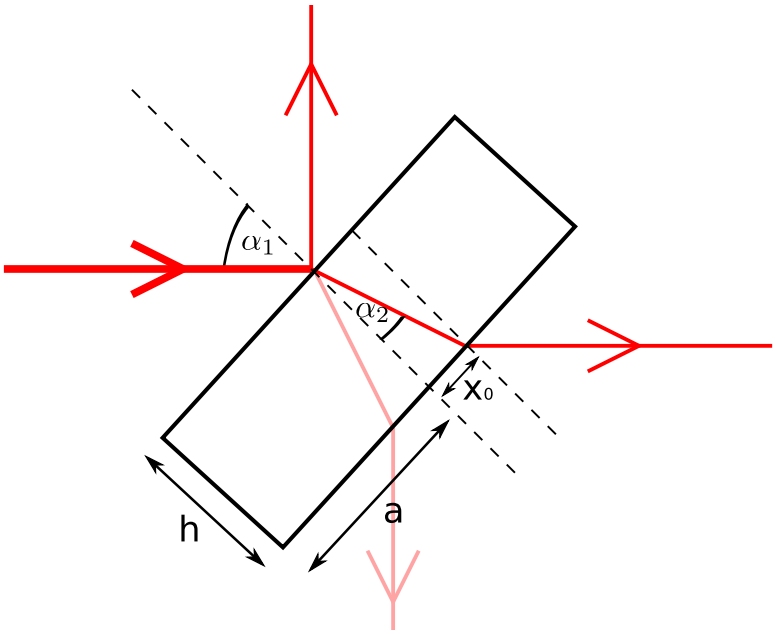


Figure 4: Central aLIGO beam splitter geometry. The different beams are shown and their points of incidence at the front and back surface.

## 3.1 Direct clipping at the central beam splitter

The size of the beam, compared with the size of the optic, is largest at the central beam splitter. The beam splitter is therefore a suitable point to begin our investigation into the effects of clipping on the observed power build-up.

### 3.1.1 Beam splitter dimensions

Figure 4 shows a diagram of the central beam splitter and the relevant dimensions. The incoming beam hits the beam splitter at 45° and travels through the beam splitter substrate at an angle of:

$$\alpha_2 = \sin^{-1}\left(\frac{1}{1.44963}\sin\left(45°\right)\right) = 29.195° \tag{1}$$

The thickness, $h$, of the beam splitter is 6 cm, so the beam travels a length of:

$$\delta L = \frac{6\text{ cm}}{\cos\left(\alpha_2\right)} = 6.873\text{ cm} \tag{2}$$

inside the beam splitter. The beam exits the beam splitter slightly off-centre. Assuming the incoming beam is incident on the centre of the optic this offset is:

$$x_0 = h\tan\left(\alpha_2\right) = 3.35\text{ cm} \tag{3}$$

The BS has an overall aperture diameter of $2a = 37$ cm.

### 3.1.2 Front surface

At the beam splitter the beam appears elliptical in the frame of the mirror, due to the non-normal incidence of the beam. To calculate the elliptical aperture at which 1 ppm clipping occurs the clipping radius for $x$ and $y$ were separately calculated using a Matlab function, `FT_find_radius_for_clipping_loss`, which uses an analytical calculation that calculates the clipping, `FT_LG_clipping_loss` and an `fminsearch` to find the radius [13]. The separate radii for $x$ and $y$ are used as the axes for the elliptical aperture. The clipping by the beam splitter

is calculated by creating a mask in the shape of the beam splitter aperture, appyling this to the incident light field and calculating `1-FT_power_in_field(field,x,y)`. This method is also used to check that the clipping by the 1 ppm ellipse is actually 1 ppm.

The direct clipping at the front of the beam splitter is summarised in table 1, comparing that for the design parameters with that for the current beam-sizes in our as-built model (with compensation of ITMX to $R_c = 1901.5\,\text{m}$ for optimum mode-matching, see figure 2). Figure 5 shows the amplitude of these two beams at the beam splitter, comparing the corresponding 1 ppm clipping aperture with the aperture created by the front of the beam splitter. The larger beam from the current model incurs greater clipping and in both cases the clipping at the front surface happens primarily along the $x$-axis, as the aperture is effectively smaller due to the 45° incident angle.

| $w_x$ [cm] | $w_y$ [cm] | Clipping [ppm] |
|---|---|---|
| 5.3 | 5.3 | 1 |
| 6.6 | 7.1 | 120 |

Table 1: Summary of beam sizes and direct clipping on the front of the beam splitter. The first set of numbers refer to design parameters. The second set refer to our current as-built model, with the radius of curvature of ITMX tuned to match the beam sizes of PRX and PRY (ITMX $R_c = 1901.5\,\text{m}$, see figure 2).

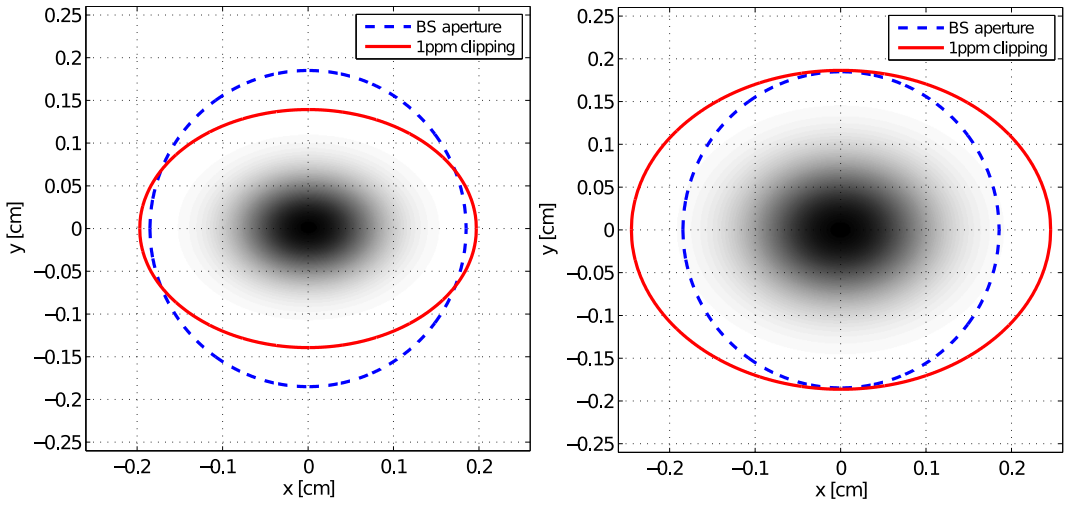


Figure 5: Beam amplitude on the front of the central beam splitter. Left: design parameters ($w = 5.3\,\text{cm}$). Right: as-built parameters with ITMX $R_c$ tuned to 1901.5 m for optimum mode-matching between the arms ($w_x = 6.6\,\text{cm}$, $w_y = 7.1\,\text{cm}$, see figure 2). The beam is shown as the projection onto the BS surface and so appears strongly elliptical. The aperture of the BS and the aperture which would achieve 1 ppm clipping are shown.

### 3.1.3 Back surface

At the back surface the incident beam is slightly off-centre (3.35 cm) but the aperture diameter remains the same. This clipping at the back of the beam splitter (table 2) is significantly greater than at the front, around 1 order of magnitude. The offset of the beam on this surface also introduces some anti-symmetric clipping of the beam (figure 6). The clipping at the beam splitter is dominated by the centering on the back surface and overall the current as-built model suggests an increase in clipping > an order of magnitude, compared with the original design.

| $w_x$ [cm] | $w_y$ [cm] | Clipping [ppm] |
|---|---|---|
| 5.3 | 5.3 | 35 |
| 6.6 | 7.1 | 840 |

Table 2: Summary of beam sizes and clipping at the back of the beam splitter. The first set of numbers refer to design parameters. The second set refer to the LLO as-built model, with ITMX $R_c$ tuned to match the beam sizes of PRX and PRY (ITMX $R_c = 1901.5\,\mathrm{m}$, see figure 2).

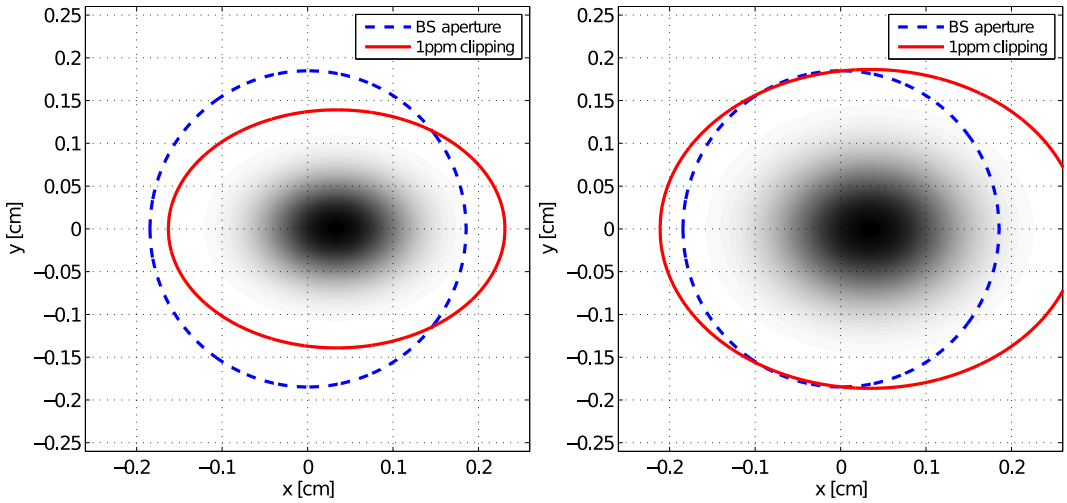


Figure 6: Beam amplitude on the back of the central beam splitter. Left: design parameters ($w = 5.3\,\mathrm{cm}$). Right: as-built parameters with ITMX $R_c$ tuned to 1901.5 m for optimum mode-matching between the arms ($w_x = 6.6\,\mathrm{cm}$, $w_y = 7.1\,\mathrm{cm}$, see figure 2). The beam is shown as the projection onto the BS surface, including the expected offset of the beam according to the BS geometry (figure 4). The aperture of the BS and the aperture which would achieve 1 ppm clipping are shown.

## 3.2 Power-recycled Michelson with thermal compensation

The clipping at the beam splitter was calculated for optimum mode-matching between the two arms (ITMX $R_c = 1901.5\,\mathrm{m}$) which is achieved when the thermal compensation systems are running. For the cold state the eigenmode of PRX will have a smaller beam (see figure 2) and the clipping will be slightly smaller. However, the mode-matching between the arms will be worse.

Figure 7 shows the power recycling gain as the curvature of ITMX is adjusted, mimicking the effects of the thermal compensation system. Including the effects of the aperture on the front of the beam splitter has little effect. However, adding the aperture on the back of the beam splitter significantly reduces the optimum power recycling gain achievable, even when optimum mode-matching is achieved. The point of maximum gain is shifted from the case where the aperture effects are ignored, effectively optimising between good mode-matching and minimal clipping. Figure 7 also shows the corresponding contrast defect, which is minimised when the mode-mismatch is minimised (ITMX $R_c = 1901.5\,\mathrm{m}$). This goes some way to explaining the discrepancy between the observed maximum PRC gain and minimum contrast defect observed on site (figure 1). Figure 7 also shows the PRC gain and contrast defect for the case with our as-built optical layout but using an injected laser beam which is mode-matched to the initial IFO design, i.e. the beam we might expect from the input optics. In this case the eigenmodes of the cavities formed between PRM and the two ITMs still have too large beams at the BS and the mode-matching between the input beam and the power recycling cavity is now worse, resulting in less power initially injected into the interferometer.

Figure 8 shows the power recycling gain as the radii of curvature of both ITMX and ITMY are adjusted, taking into account the BS apertures on the front and back surface. As was observed experimentally (figure 1) the thermal correction of both ITMX and ITMY can lead to very low power build-up.

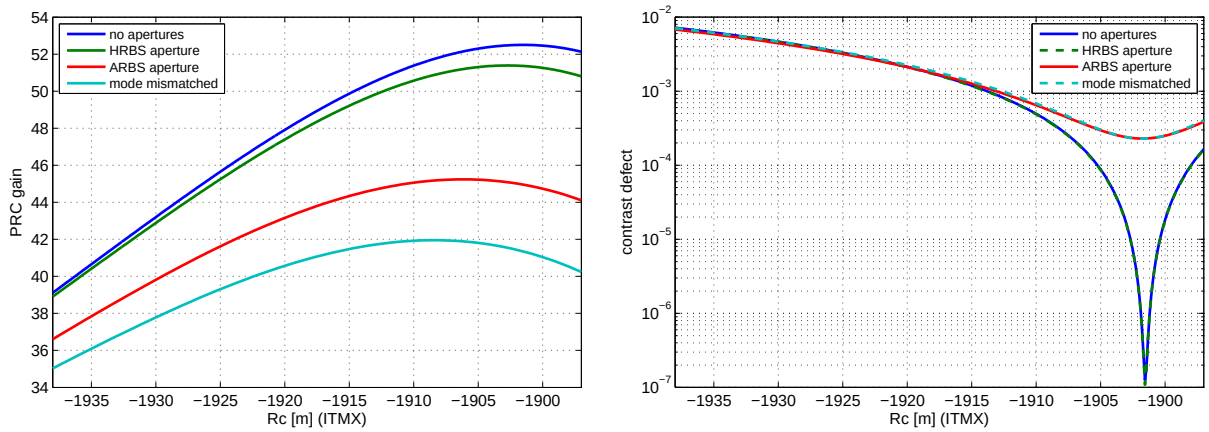


Figure 7: Power recycling gain (left) and contrast defect (right) as the radius of curvature of ITMX is tuned in our as-built PRMI model (LLO). Optimum mode-matching occurs at $\sim -1901.5$. Four different cases are simulated: 1) no apertures applied; 2) aperture applied to the front (HR) side of the beam splitter; 3) apertures applied to the front and back (AR) side of the BS; 4) apertures applied to both sides of the BS and simulated with a mode-mismatched input beam (using the ideal beam for the original design). All other optics parameters are as specified in 1.3. Cases 3 and 4, showing a significant drop in PRC gain and a discrepancy between maximum gain and minimum contrast defect go some way to understanding the observed results (figure 1).

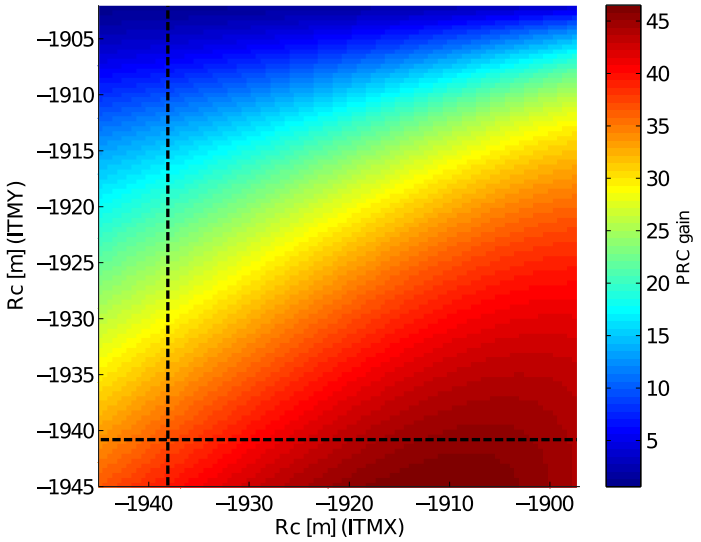


Figure 8: Power recycling gain for different ITMX/Y radii of curvature in the current PRMI model, including the apertures created by the two faces of the BS. The change in curvature represents the action of the TCS ring heaters and the dashed lines mark the measured $R_c$s of the cold optics [11]. The input beam is mode-matched to the cavity formed between the PRM and ITMY. All other optics parameters are as specified in 1.3. By actuating the curvature of both ITMX and ITMY it is possible to cause a significant drop in PRC gain, as observed at LLO (figure 1).

### 3.3 Optimum beam centring

The sensitivity of the power buildup to the aperture created by the back of the beam splitter is primarily due to the off-centring of the beam on the back surface. Figure 9 shows the power build up as the beam position on the optic is shifted from the centre (of the front surface). By shifting the beam across the beam splitter the PRC gain can be maximised, optimising between clipping at the front face and clipping at the back during X arm transmission. However, at this point the clipping on the back face into the signal recycling cavity will become much worse as this beam is shifted further towards the BS edge.

Just small offsets ($\sim$1 cm) in the wrong direction can significantly impact the power build up. This effect is more pronounced in our current model (than in the design) due to the larger beam sizes at the beam splitter. Figure 9 shows two different cases. The mode-matched case has the two arms matched by actuating on the ITMX curvature ($R_c = 1901.5$ m) and a mode-matched input beam. This case can reach a maximum PRC gain of 48 with a steep drop in gain when the BS is off-centred. The mode-mismatched case, using matched arms but with a mode-mismatched input beam, can reach a maximum of $\sim 45$.

### 3.4 Uncertainties in power recycling cavity parameters

In section 2.2 the effect of uncertainties in parameters of the power recycling cavity was seen to have a large effect on the beam size at the beam splitter. Figure 10 shows the effect that errors in the radius of curvature of PR3 would have on the power buildup, when the beam splitter apertures are included. The dramatic increase in beam-size caused by just small changes to PR3 $R_c$ can lead to large changes in the PRC gain. Even changes on the order of a cm could lead to a drop in PRC gain $> 10$. Similar changes in gain are seen for small changes ($\sim 5$ mm) in the distance between PR2 and PR3. While this helps explain the low power buildup seen at L1 (figure 1 it also implies that replacing PR3 with a mirror with a slightly smaller radius of curvature, or adjusting the distance between PR2 and PR3, could increase the power recycling gain, by reducing the beam-size at the BS. Potentially, by combining this with the thermal compensation system we could recover gains $> 50$ with the current ITMs. Figure 10 shows the gain for two cases, mode-matched between the two arms and the input beam and mode-mismatched, with balanced arms but a mode-mismatched input beam. This gives a range of

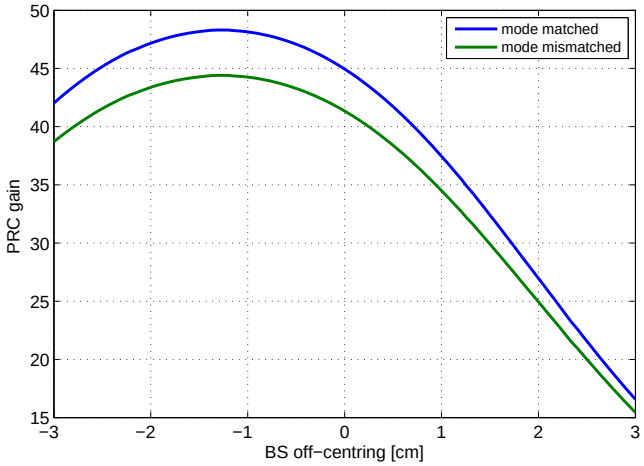


Figure 9: Potential gain in the power recycling cavity as the incident beam position is shifted across the front surface of the beam splitter in the current PRMI model, including BS apertures (front and back). Two cases are considered: 1) a mode-matched case, with optimal mode matching between the arms (ITMX $R_c = 1901.5\,\mathrm{m}$, see figure 2) and an input beam mode-matched to the PRC; 2) a mode-mismatched case, using the matched arms and a mismatched input beam (using the ideal beam for the original design). All other optics parameters are as specified in 1.3. The PRC gain can be optimised by off-centering on the BS but at the expense of a loss of signal into the signal recycling cavity.

possible PRC gains.

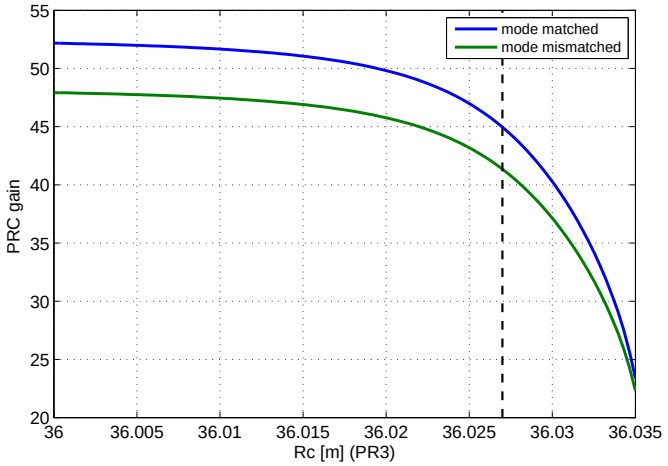


Figure 10: Gain in the power recycling cavity when the radius of curvature of PR3 is tuned in the current PRMI model for LLO, including BS apertures. The dashed line refers to the measured $R_c$ of PR3 [11] used in current simulations. Two cases are considered: 1) a mode-matched case, with optimal mode matching between the arms (ITMX $R_c = 1901.5\,\mathrm{m}$, see figure 2) and an input beam mode-matched to the PRC; 2) a mode-mismatched case, with mode-matched arms and a mismatched input beam (using the ideal beam for the original design). All other optics parameters are as specified in 1.3. The steep drop in PRC gain is a result of the increased clipping which occurs when the beam size increases with PR3 $R_c$ (see figure 3).

### 3.5 Clipping at baffles

In reality the beam-splitter includes baffles at both the front and back which will clip the beam even further. In our initial investigation we focused on the natural apertures caused by the beam-splitter for simplicity when investigating the general behaviour of the interferometer in the presence of clipping at the BS.

Our final simulation includes the baffles on all faces of the beam splitter, representing these using absorption maps. The baffle geometry is as described in [14, 15, 16, 17]. Figure 11 shows the final result, where the radius of curvature of ITMX is tuned with the baffles applied to the beam-splitter. The PRC gain ranges between 30 and 36, very similar to the values measured in the experiment (figure 1).

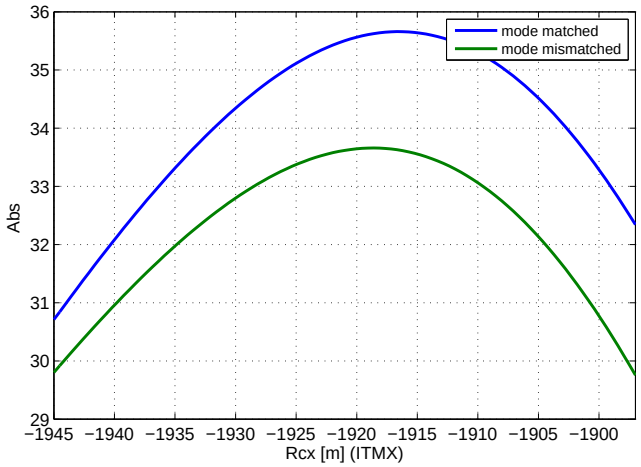


Figure 11: Gain in the power recycling cavity as ITMX $R_c$ is tuned, with baffles applied to the front and back of the beam-splitter. The maximum in PRC gain is much lower than the design prediction of 57 and the maximum has shifted from the point of optimum mode-matching between the two arms (ITMX $R_c = 1901.5$). The cases for an input beam mode-matched to PRY and a mode-mismatched input beam (matched to the original L1 design) are shown. These values should be compared with the experimental result (figure 1).

### 3.6 Conclusion

The observed power recycling gain at L1 (figure 1) can be explained by greater than expected clipping at the central beam splitter, due to larger beam sizes than the original design. The positioning and radius of curvature of certain power recycling optics, namely PR3 $R_c$ and the distance between PR2 and PR3, affect the size of the beam and any uncertainties in these could result in a dramatic change in the clipping and power recycling gain.

Adding in the ETMs will have an impact on the beam sizes within the interferometer. Not only will the beams circulating in the arms have an effect on the overall beam-size at the beam splitter, but the additional build up of power will lead to thermal lensing in the ITMs, negating the negative lens in the current ITMY and changing the eigenmodes of PRX/Y. Therefore the beam-sizes in the full interferometer are likely to be different than those modelled here. However, care should be taken with the positioning of PR2 and PR3 to avoid too large a beam at the beam splitter and a large power loss in the full interferometer.

# Appendix

# A ITM susbtrate non-thermal lens calculation

The polisher data gives the value for the wave front radius of curvature measured in reflection from the ITM HR surface when probed from the AR side of the optic, less the expected wave front radius of curvature calculated from the measured radius of curvature of the HR surface. Several steps are required to get from this measurement value to the equivalent ITM lens focal length value.

| Optic number | Location | HR Rc (vendor) [m] | HR Rc (LIGO) [m] | Measured wave-front error [m] | Calculated lens focal length [m] |
|---|---|---|---|---|---|
| ITM 01 | CIT | 1939.32 | NA | -9.46 | -92780 |
| ITM 03 | LMA (to H1 Y) | 1939.52 | NA | -10.92 | -80213 |
| ITM 04 | L1 X | 1938.61 | 1937.9 | 2.93 | 304989 |
| ITM 05 | CIT | 1939.18 | NA | 11.56 | 78347 |
| ITM 06 | CIT | 1937.6 | NA | 2.34 | 381154 |
| ITM 07 | CIT | 1938.53 | NA | -2.85 | -310812 |
| ITM 08 | L1 Y | 1938.44 | 1940.7 | -10.62 | -82424 |
| ITM 09 | H1 X (temp) | 1938.15 | NA | 3.9 | 229357 |
| ITM 10 | CIT | 1938.15 | NA | -9.37 | -93570 |
| ITM 11 | LMA (to H1 X) | 1939.39 | NA | 1.56 | 572117 |

Table 3: Table of geometric propetries of aLIGO ITMs. The ITM non-thermal lens substrate focal lengths are calculated using the method described in this appendix.

First of all, we calculate the expected value for the wave-front radius of curvature in reflection from the ITM HR surface via the AR surface at the polisher's measurement wavelength of 633 nm (HeNe laser).

$$^{\mathrm{HeNe}}Rc^{\mathrm{expected}}_{\mathrm{wavefront}} = \frac{Rc_{\mathrm{HR}}}{2\mathrm{n}_{\mathrm{HeNe}}} \tag{4}$$

The measurement is made using a HeNe laser, so we use the refractive index of suprasil at 633 nm: $\mathrm{n}_{\mathrm{HeNe}}$ =1.457. Adding the value for 'transmitted reflected wave-front curvature' $\delta Rc^{\mathrm{wave}}$ as quoted in the polisher's reports [6, 7] gives the measured value for the wave-front radius of curvature of 633nm light in reflection from the ITM HR surface via the AR surface:

$$^{\mathrm{HeNe}}Rc^{\mathrm{measured}}_{\mathrm{wavefront}} = ^{\mathrm{HeNe}}Rc^{\mathrm{expected}}_{\mathrm{wavefront}} + ^{\mathrm{HeNe}}\delta Rc^{\mathrm{wave}} \tag{5}$$

We then convert from the measured wavefront curvature with the HeNe laser to the wavefront curvature that would be seen by a Nd:YAG laser at 1064 nm:

$$^{\mathrm{Nd:YAG}}Rc^{\mathrm{measured}}_{\mathrm{wavefront}} = ^{\mathrm{HeNe}}Rc^{\mathrm{measured}}_{\mathrm{wavefront}} \frac{\mathrm{n}_{\mathrm{HeNe}}}{\mathrm{n}_{\mathrm{Nd:YAG}}} \tag{6}$$

We can find the expected wavefront radius of curvature at 1064 nm in the same way as we did for the 633 nm case:

$$^{\mathrm{Nd:YAG}}Rc^{\mathrm{expected}}_{\mathrm{wavefront}} = \frac{Rc_{\mathrm{HR}}}{2\mathrm{n}_{\mathrm{Nd:YAG}}} \tag{7}$$

Now we know the difference in expected and measured wavefront curvatures at 1064 nm. We just have to solve for the optical power that would give us this curvature difference:

$$P = \frac{1}{^{\mathrm{Nd:YAG}}Rc^{\mathrm{measured}}_{\mathrm{wavefront}}} - \frac{1}{^{\mathrm{Nd:YAG}}Rc^{\mathrm{expected}}_{\mathrm{wavefront}}} \tag{8}$$

Bearing in mind that this optical power is attributed to the light during a double-pass of the ITM substrate lens, the ITM lens focal length may now be calculated as:

$$f^{\mathrm{ITM}}_{\mathrm{sub}} = \frac{2}{P} = 2\left(\frac{1}{^{\mathrm{Nd:YAG}}Rc^{\mathrm{measured}}_{\mathrm{wavefront}}} - \frac{1}{^{\mathrm{Nd:YAG}}Rc^{\mathrm{expected}}_{\mathrm{wavefront}}}\right)^{-1} \tag{9}$$

Table A shows the ITM susbtrate non-thermal lens focal lengths calculated in this way, along with other measured geometrical properties, for several of the ITM optics listed in [11].

# References


[1] A. Freise, G. Heinzel, H. Lück, R. Schilling, B. Willke, and K. Danzmann, "Frequency-domain interferometer simulation with higher-order spatial modes," Class. Quantum Grav. **21**, S1067 (2004), the program is available at http://www.gwoptics.org/finesse 1

[2] LLO aLOG 9333, Denis Martynov, 25.10.2013, https://alog.ligo-la.caltech.edu/aLOG/index.php?callRep=9333 1

[3] LLO aLOG 9733, Chris Mueller, 15.11.2013, https://alog.ligo-la.caltech.edu/aLOG/index.php?callRep=9733 2, 3

[4] LLO aLOG 8192, Lisa Barsotti, 07.08.2013, https://alog.ligo-la.caltech.edu/aLOG/index.php?callRep=8192 1

[5] LIGO-G1300909, 'Mode matching investigations at LLO', Chris Mueller and Lisa Barsotti, https://dcc.ligo.org/LIGO-G1300909 1

[6] LIGO-C1000472-v2, 'ITM04 Input Test Mass Final Polishing Data Package', Garrilynn Billingsley, 23.05.2010, https://dcc.ligo.org/C1000472 1, 4, 13

[7] LIGO-C1000476-v2, 'ITM04 Input Test Mass Final Polishing Data Package', Garrilynn Billingsley, 23.05.2010, https://dcc.ligo.org/C1000476 1, 4, 13

[8] LIGO-T1300901, 'Finesse input files for the L1 interferometer', Charlotte Bond, Paul Fulda, Andreas Freise, Daniel Brown, Keiko Kokeyama, Ludovico Carbone, 13.11.2013, https://dcc.ligo.org/LIGO-T1300901 3

[9] LIGO-T0900043, 'Optical Layout and Parameters for the Advanced LIGO Cavities', Muzammil Arain, 16.03.2012, https://dcc.ligo.org/LIGO-T0900043 4, 5

[10] LIGO-T1100034, 'aLIGO Final Design of Ring Heaters and Electronics', Mindy Jacobson, 19.05.2011, https://dcc.ligo.org/LIGO-T1100034 4

[11] LIGO core optics reference page, https://nebula.ligo.caltech.edu/optics/ 3, 5, 10, 11, 13

[12] LIGO-E1200274-v3, 'ALIGO IO L1 MASTER COORDINATE LIST', Luke Williams, 04.12.2012, https://dcc.ligo.org/E1200274 3

[13] Simtools, a collection of Matlab tools for optical simulations, http://www.gwoptics.org/simtools/ 6

[14] LIGO-D1200750, 'aLIGO, AOS, BS elliptical baffle ASST', Kurt Buckland, 2012, https://dcc.ligo.org/LIGO-D1200750 12

[15] LIGO-D1200703, 'aLIGO, AOS, BS X elliptical baffle', Kurt Buckland, 2012, https://dcc.ligo.org/LIGO-D1200703 12

[16] LIGO-D1200704, 'aLIGO, AOS, BS Y elliptical baffle', Kurt Buckland, 2012, https://dcc.ligo.org/LIGO-D1200704 12

[17] LIGO-T1000090, 'Advanced LIGO baffle design using SIS', Hiro Yamamoto, 2012 https://dcc.ligo.org/LIGO-T1000090 12